JEM Journal of Experimental Medicine

ARTICLE

Neuraminidase inhibition contributes to influenza A virus neutralization by anti-hemagglutinin stem antibodies

Ivan Kosik[1], Davide Angeletti[1], James S. Gibbs[1], Matthew Angel[1], Kazuyo Takeda[2], Martina Kosikova[3], Vinod Nair[4], Heather D. Hickman[5], Hang Xie[3], Christopher B. Brooke[6], and Jonathan W. Yewdell[1]

Broadly neutralizing antibodies (Abs) that bind the influenza virus hemagglutinin (HA) stem may enable universal influenza vaccination. Here, we show that anti-stem Abs sterically inhibit viral neuraminidase (NA) activity against large substrates, with activity inversely proportional to the length of the fibrous NA stalk that supports the enzymatic domain. By modulating NA stalk length in recombinant IAVs, we show that anti-stem Abs inhibit virus release from infected cells by blocking NA, accounting for their in vitro neutralization activity. NA inhibition contributes to anti-stem Ab protection in influenza-infected mice, likely due at least in part to NA-mediated inhibition of FcγR-dependent activation of innate immune cells by Ab bound to virions. Food and Drug Administration–approved NA inhibitors enhance anti-stem–based Fc-dependent immune cell activation, raising the possibility of therapeutic synergy between NA inhibitors and anti-stem mAb treatment in humans.

Introduction

The severe 2017–2018 influenza season provided a timely if unwelcome reminder of the limitations of current vaccines in coping with antigenic drift in the viral surface proteins hemagglutinin (HA) and neuraminidase (NA). HA mediates viral attachment to cell-surface sialic acid (SA) residues and subsequent fusion of viral and cellular membranes. NA releases nascent virus from infected cells by removing terminal sialic residues from glycoproteins and glycolipids.

Current vaccines induce antibodies (Abs) specific for the HA head. Head-binding Abs neutralize influenza A virus (IAV) infectivity in vitro by blocking virus attachment and, depending on the epitope recognized, preventing the conformational alterations needed to trigger membrane fusion. Due to the immunodominance of the HA head following infection and standard vaccination, Ab responses drive rapid evolution in the head that enables viral escape. In contrast to the HA head, the stem domain is highly conserved and cross-reactive between strains within the same group. Early proof-of-principle studies found that a stem-specific mAb could block HA-mediated fusion, neutralize IAV, and protect against IAV disease in animal models (Styk et al., 1979; Russ et al., 1987; Okuno et al., 1993, 1994). Further studies from many laboratories indicated that broadly neutralizing (BN) stem-specific Abs are common in humans and can be induced by standard vaccination protocols, albeit at low levels relative to head-specific Abs (Chiu et al., 2015; Henry Dunand and Wilson, 2015; Corti et al., 2017). Much more robust BN stem-specific responses can be elicited by native stem-only immunogens (Lu et al., 2014; Mallajosyula et al., 2014; Impagliazzo et al., 2015; Yassine et al., 2015) or a prime-boost head–stem chimeric HA molecule strategy (Krammer et al., 2018).

Although Ab-driven antigenic drift in the stem may ultimately limit stem-based vaccination (Lees et al., 2014; Doud et al., 2018), as a promising "universal" vaccine strategy, it is critical to understand the mechanisms of anti-stem Abs in reducing or preventing IAV disease in humans. Stem-binding Abs have been reported to block viral entry into cells by preventing the acid-induced conformations alterations in HA required to catalyze viral–cell membrane fusion (Varecková et al., 2003) and prevent release from infected cells through an unknown mechanism (Yamayoshi et al., 2017). In vivo, anti-stem Abs may largely exert protection via

[1]Cellular Biology Section, Laboratory of Viral Diseases, National Institute of Allergy and Infectious Diseases, Bethesda, MD; [2]Microscopy and Imaging Core Facility, Center for Biologics Evaluation and Research, Food and Drug Administration, Silver Spring, MD; [3]Laboratory of Respiratory Viral Diseases, Division of Viral Products, Office of Vaccines Research and Review, Center for Biologics Evaluation and Research, Food and Drug Administration, Silver Spring, MD; [4]Electron Microscopy Unit, Research Technologies Branch, Rocky Mountain Laboratories, National Institute of Allergy and Infectious Diseases, National Institutes of Health, Hamilton, MT; [5]Viral Immunity and Pathogenesis Unit, Laboratory of Clinical Immunology and Microbiology, National Institute of Allergy and Infectious Diseases, Bethesda, MD; [6]Department of Microbiology, University of Illinois, Urbana, IL.

Correspondence to Jonathan W. Yewdell: jyewdell@niaid.nih.gov.

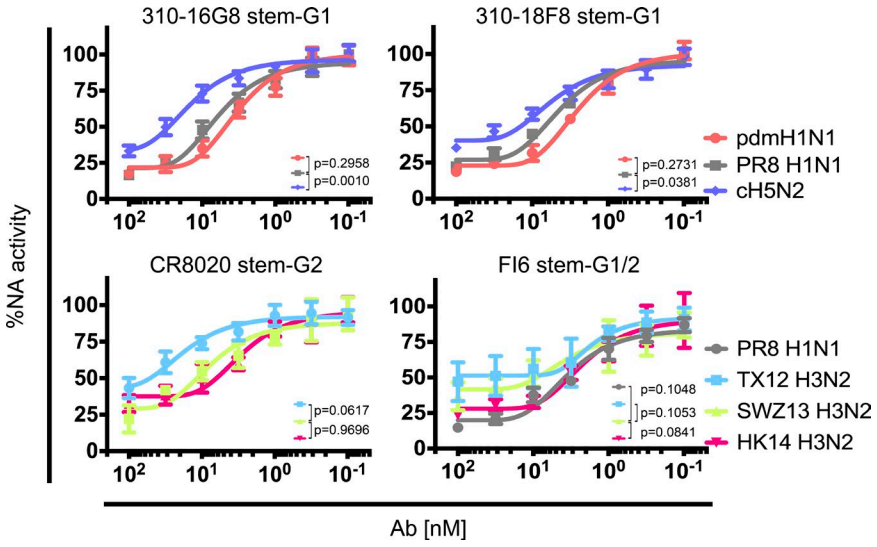

Figure 1. **BN anti-HA stem mAbs sterically block NA activity.** We measured the capacity of purified anti-stem mAbs on NA activity via ELLA against the viruses indicated. ELLA is based on NA removal of terminal SAs from plate-bound fetuin, which is assessed by binding of a lectin for the exposed penultimate galactose. mAbs used are specific for either group 1 (G1) or group 2 (G2) HA stems or bind both groups (G1/2). We normalized data by NA activity in the absence of the Ab (set to 100%). Error bars indicate the SD of duplicate samples acquired in three independent experiments (n = 6). One-way ANOVA with Dunnett's multiple comparisons was performed on the IC_{50} (calculated for independent experiments) to determine statistical significance (top panels against PR8 H1N1, and bottom panels against SWZ13 H3N2), and P values are indicated in the panels.

Fc-mediated activation of humoral and cellular innate immune functions (DiLillo et al., 2014; Cox et al., 2016).

HA is typically present on virions at more than fivefold higher molar amounts than NA. Abs specific for the HA globular and stem domains can sterically interfere with NA activity against large protein substrates as long as virus remains intact (Russ et al., 1974; Kosik and Yewdell, 2017; Rajendran et al., 2017), suggesting a possible mechanism for stem Ab–mediated inhibition of viral release from infected cells. Here, we show that NA inhibition (NAI) can be a major contributor of BN activity of stem-specific Abs in vitro and in vivo, in the latter case likely by interfering with Fcγ receptor–activated innate immune cell antiviral effector activity.

Results

BN HA stem–specific mAbs inhibit viral NA

The commonly used enzyme-linked lectin assay (ELLA) method for measuring Ab-mediated NAI is complicated by blockade of viral access to the plate-bound substrate by anti-HA head Abs that block viral attachment (Kosik and Yewdell, 2017). This does not, however, apply to stem-binding Abs, which do not block virus attachment even at saturating concentrations (Fig. S1 A). Anti-stem mAbs 310-16G8 and 310-18F8 (Whittle et al., 2014) efficiently inhibit N1 or N2 NAs using viruses with H1 HA stems (PR/8/34 [H1N1], Cal/4/09 [H1N1], and chimeric cH5/1N2 [H5-head-H1-stem N2]; Fig. 1). They fail, however, to inhibit the N2 NA on HK68, which possesses an H3 HA not recognized by these group 1–specific mAbs (Fig. S1 C). By contrast, CR8020 and FI6 mAbs, which bind group 2 and both group 1 and 2 stems, inhibit NA activity of multiple group 2 viruses, demonstrating that NAI can be mediated by a group I/II cross-reactive stem-specific Ab (Fig. 1).

How efficient is this phenomenon? We compared the NAI activity of NA2-10E10, an NA-specific mAb, to 310-16G8 and 310-18F8. After normalizing Ab concentrations to account for the different avidities of the mAb, the HA and NA Abs exhibit similar NAI activities (Fig. S1 E). Interestingly, while NA2-10E10 nearly completely inhibited NA activity, at saturation, the HA stem–specific mAbs failed to inhibit 15–25% of NA activity. This suggests the geometric relationship of NA relative to HA may govern the maximal extent of cross-spike inhibition.

As with globular domain–specific mAbs (Kosik and Yewdell, 2017), NAI with stem-binding Abs was abrogated using detergent-treated virus, illustrating the steric nature of inhibition (Fig. S1 B).

NAI of stem-specific Abs is inversely related to NA stalk length

Curiously, the chimeric H5/1N2 virus exhibits two- to threefold increased resistance to stem mAb–mediated NAI compared with PR8, despite sharing the identical stem sequence (Fig. 1). Sequence alignment of the relevant N1 and N2 NAs revealed a 15–amino acid extension in the N2 NA stalk region (Fig. S1 F), suggesting that NA stalk length may influence the NAI activity of anti-stem Abs. The NA stalk exhibits natural length variability (Li et al., 2011), and its modulation is frequently associated with host adaptation and pathogenicity changes (Matsuoka et al., 2009; Sun et al., 2013; Bi et al., 2015).

To examine the influence of NA stalk length on anti-stem Ab function, we generated recombinant PR8 viruses with NAs lacking a stalk (del24) or with a 20-residue insertion (ins20; Fig. S2 A). Despite no obvious differences in the morphology of purified virions by cryo-electron microscopy (cryo-EM; Fig. S2 B), immunoblotting for NA confirmed the expected alteration in molecular mass in SDS-PAGE (Fig. S2 C). Using two independently generated recombinant virus preparations, we found that WT, del24, and ins20 purified virions contained similar amounts of NA and HA by quantitative immunoblotting (Fig. S2 C). Kinetic analysis of NA activity in purified viruses using the small fluorogenic substrate 4-methylumbelliferyl-a-D-N-acetylneuraminic acid (MUNANA; Table S1) revealed that adding or deleting stalk amino acids had minor effects on NA maximal enzyme velocity (V_{max}) or the Michaelis–Menten constant (K_m). By contrast, lengthening the stem greatly accelerated NA-mediated release from RBCs while shortening the stem-retarded release (Fig. S2 D), confirming previous findings (Chockalingam et al., 2012). While ins20 and del24 exhibit altered release from RBCs compared with WT, all the viruses replicated with similar kinetics in Madin-Darby Canine Kidney

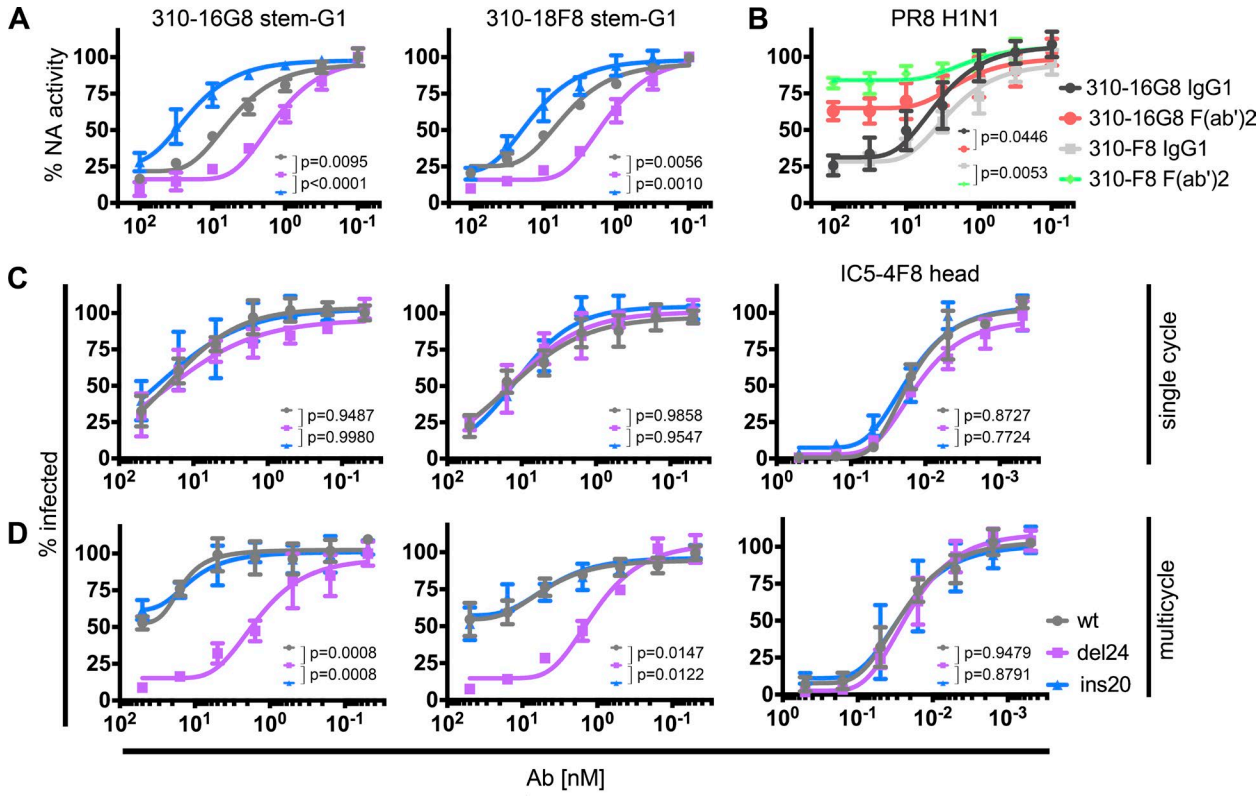

Figure 2. **Stalk length governs anti-stem Ab NAI and multicycle VN activity. (A)** NAI activity of the indicated purified mAbs determined by ELLA, as in Fig. 1, using wt PR8 and mutants with 20 residues added to the NA stalk (ins20) or a completely deleted NA stalk (del24). Error bars indicate the SD of duplicate samples acquired in three independent experiments (n = 6). **(B)** Comparison of the NAI activity of the indicated purified mAbs and their respective F(ab')2 fragments using PR8. Error bars indicate the SD of duplicate samples acquired in two independent experiments (n = 4). **(C)** VN activity of the indicated purified mAbs determined by incubating mAbs with the mCherry reporter viruses indicated before adding to MDCK SIAT1 cells and after 4–5 h, quantitating infected cells by flow cytometry to detect mCherry expression. Data are normalized with 100% set as the fraction of infected cells in the absence of Ab. Error bars indicate the SD of duplicate samples acquired in three independent experiments (n = 6). **(D)** As in C, but measuring infected cells 18 h p.i. to allow multicycle infection. Error bars indicate the SD of duplicate samples acquired in three independent experiments (n = 6). One-way ANOVA with Tukey's multiple comparisons was performed on the IC_{50} or areas under the curves (calculated for independent experiments), and P values are indicated in the panels.

(MDCK) SIAT1 cells, consistent with similar replication also in vivo (Fig. S2 D).

We next examined HA stem Ab–mediated NAI using the stalk mutants. Using ELISA, we established that NA stalk length does not affect the binding of anti-HA stem mAbs 310-16G8 and 310-18F8 to plate-bound purified virus (Fig. S3, top). Similarly, flow cytometry revealed that the NA stalk does not affect stem Ab binding to HA on infected MDCK cells (Fig. S3). Despite this, shortening the NA stalk increased the NAI activity of the same mAbs by approximately fourfold relative to WT virus, while lengthening the stalk had the opposite effect, resulting in a 10- to 20-fold difference in NAI titers in ins20 versus del24 viruses (Fig. 2 A). Consistent with a steric mechanism of NAI, removal of the Fc portion (50 kD) of the anti-stem Ab reduced their NAI activity (Fig. 2 B). Importantly, the median inhibitory concentration (IC_{50}) values of the F(ab')2 fragments were lower (i.e., more efficient) than the intact Abs (310-16G8 intact, 4 nM; F(ab')2, 1.7 nM; F8 intact, 2.6 nM; F(ab')2, 1.9 nM), but the NA-resistant fraction increased two- to threefold. This is consistent with the idea that the geometry of the HA and NA on the virion creates populations of HA that vary in the steric effects of bound anti-stem Abs.

NAI contributes to virus-neutralizing (VN) activity of stem-specific Abs by inhibiting release

Our findings predict that stem-binding Abs should neutralize viral infectivity by inhibiting NA-mediated release from infected cells. To test this prediction, we examined the effect of NA stalk length on mAb neutralization. For this, we generated a panel of reporter viruses that express mCherry, enabling precise flow cytometric enumeration of virus-infected cells. We added virus preincubated with mAbs at 37°C to MDCK SIAT1 cells and measured frequency of IAV infected cells 4–5 h postinfection (p.i.). IC5-4F8, a control mAb specific for the Sb antigenic site in the head domain of H1 neutralized viruses equally regardless of NA stalk (Fig. 2 C). Neutralization by two stem-specific Abs was much less efficient (even when factoring in Ab avidity) but did not vary with NA stalk length after a single replication cycle (Fig. 2 C). By contrast, when infection time was extended by 14 h to enable multicycle infection, both stem-specific mAbs demonstrated a ∼100-fold increase in neutralization against del24 relative to WT or ins20 (Fig. 2 D). This effect was stem specific, as it was not observed with IC5-4F8 (Fig. 2 D) or in the context of HK68 (Fig. S1 D).

A simple explanation for the NA-specific effect by anti-stem Abs in multistep neutralization of del24 is that anti-stem Abs block virus release, retarding cell-to-cell transmission. We therefore added mAbs 4 h after infecting MDCK-SIAT1 cells with WT, del24, or ins20 PR8 and measured NA activity of virus released into the media from cells over the next 6 h using NA activity with MUNANA as a proxy. We confirmed that mAbs did not alter the infection per se by quantitating intracellular nucleoprotein (NP) and NA in fixed and permeabilized cells by indirect immunoassay (Fig. S4). Both stem mAbs tested blocked release of each virus (Fig. 3). By contrast, the HA head-specific mAb IC5-4F8, as expected (or a control mAb specific for an irrelevant Ag), did not block virus release (Fig. 3 and Fig. S4). Importantly, both stem mAbs tested exhibited greatly enhanced effects on del24 release from cells (Fig. 3), providing an explanation for the enhanced activity of anti-HA stem Abs in the multicycle neutralization assay (Fig. 2 C).

NA stalk length controls the effectiveness of HA stem–specific Abs in limiting IAV pathogenesis

Extending these findings to an in vivo model of IAV pathogenesis, we passively transferred stem- or head-specific mAbs into C57Bl/6 mice challenged 4 h later with pathogenically equal high doses of WT or NA stalk variant viruses and monitored weight loss. Following infection without transferred Ab, 100% of mice were humanely sacrificed between day 4 and 7 p.i., when they reached >30% weight loss. As expected, mice receiving the HA head-specific mAb IC5-4F8 were efficiently protected against each virus, with minimal weight loss and 100% survival (Fig. 4 A). Surprisingly, in mice passively administered 310-16G8, infection with either WT or del24 resulted in delayed and attenuated weight loss, and all mice recovered by 10 d p.i. (Fig. 4 A). In contrast, mice infected with ins20 receiving 310-16G8 lost weight with similar kinetics as control (PBS-administered) mice, with only 17% of ins20-infected mice recovering (Fig. 4 A). Higher doses of WT virus resulted in more rapid weight loss and 100% mortality in 310-168–treated mice infected with WT virus but 80% protection and recovery by day 13 in del24-infected Ab-treated mice (Fig. 4 B).

Histological staining of lung sections on day 4 p.i. revealed less tissue destruction and immune infiltration in IC5-4F8– versus PBS-treated animals infected with each of the viruses, as expected (Fig. 5 A). There were only minor differences between WT and ins20-infected mice in terms of perivascular inflammation and bronchial epithelial damage as well as in alveolar damage and immune cell infiltration in 310-16G8–treated mice between WT and ins20 viruses (Fig. 5 A, left/right field), despite the clearly increased morbidity of ins20 infection in these mice. The only statistically significant difference in histopathological scoring was a decreased immune cell infiltration in alveoli of del24-infected mice (Fig. 5 B), clearly shown in the insets. Fluorescent immunostaining of the IAV NP in 310-16G8–treated mice mirrors alveolar histopathological burden with decreased frequency of NP-positive cells in particular for del24-infected mice (Fig. 5, C and D).

Taken together, these findings show that NA stem length, and therefore NA activity against sterically susceptible substrates, can greatly affect the in vivo activity of anti-HA stem Abs, decreasing alveolar damage in parallel with reducing virus-infected alveolar cells.

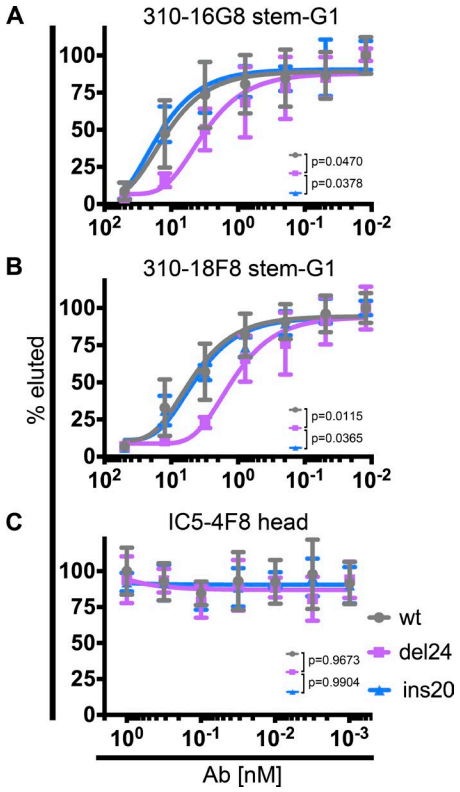

Figure 3. **Anti-stem Abs inhibit nascent virus release from infected cells. (A–C)** 4 h p.i. of MDCK SIAT1 cells with the viruses indicated, we added graded amounts of the 310-16G8 (A), 310-18F8 (B), or IC5-4F8 (C) mAbs. 6 h later, we collected the supernatant and used NA activity against a fluorescent substrate to quantitate released virions. The fluorescent signal in absence of Ab was set as 100% for each virus. Error bars indicate the SD of duplicate samples acquired in up to four independent experiments (n = 4–8). One-way ANOVA with Tukey's multiple comparisons was performed on the IC_{50} or areas under the curves (calculated for independent experiments), and P values are indicated in the panels.

NA inhibits Fc receptor–based innate cell activation

Despite the clear VN activity of anti-HA stem Abs in vitro, a number of studies indicate that their protective effect in mice depends on their interaction with Fcγ receptors (FcγR), implicating the required participation of FcγR-bearing innate immune cells (natural killer [NK] cells, macrophages, dendritic cells, and others) or/and complement (Corti et al., 2011; DiLillo et al., 2014, 2016; Sutton et al., 2017). HA stem–specific Abs are known to activate cells via FcγR interaction in a process that, in addition, requires HA binding to SA residues on the FcγR-expressing cell (DiLillo et al., 2014, 2016), since it is blocked by head-specific mAbs that block virus attachment.

We could confirm these findings using Jurkat reporter cells engineered to express luciferase after engagement of Ab-Ag complexes with the FcγRIIIa receptor expressed from a transgene (Jurkat cells are human T cell leukemia that do not naturally express Fc receptors or other NK activating receptors). Reporter cells were activated in a viral infection and stem Ab dependent manner. The addition of IC5-4F8, which binds noncompetitively

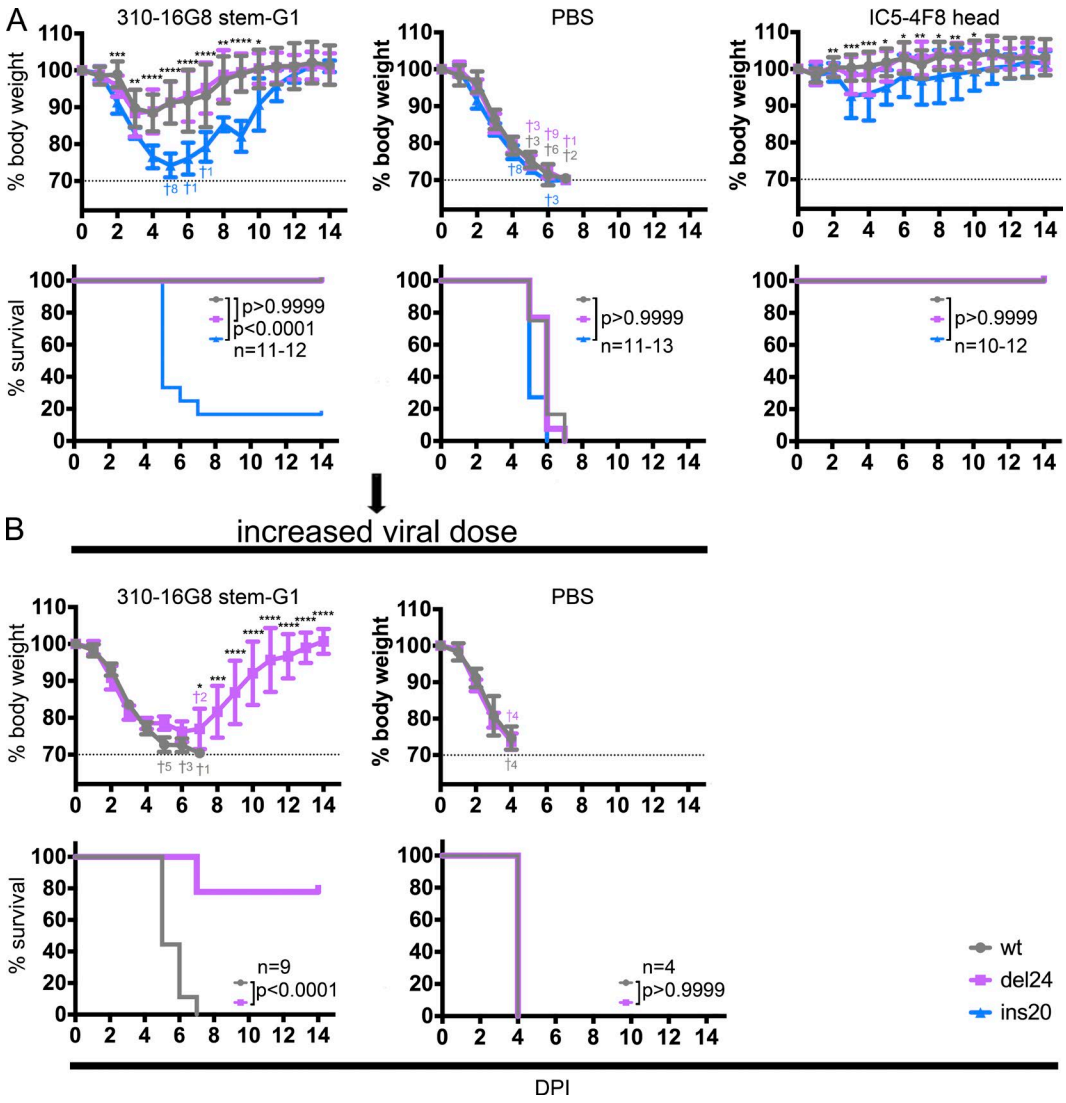

Figure 4. **Protection mediated by anti-stem Abs is dependent on NAI. (A)** We passively transferred mice (n = 10–13 mice/group, 5 mg/kg) with the stem-specific mAb 310-16G8. PBS (negative control) or head-specific mAb IC5-4F8 (positive control). 4 h after transfer, we infected mice intranasally with pathologically equal doses of WT, del24, and ins20 viruses. We monitored morbidity (body weight) and mortality (human sacrifice at >30% weight loss) for 14 d. Presented results are sum of three independent experiments (n = 3–5/group). **(B)** As in A, but with nine mice per group infected with fourfold more WT or del24 viruses. As a control, we passively transferred mice (n = 4/group) with PBS only. Error bars indicate SD. Presented results are sum of three independent experiments (n = 3–4/group). Two-way ANOVA with Bonferroni's multiple comparisons was performed to determine at which days p.i. mean weights significantly differ between the WT and ins20 groups (A) or the WT and del24 groups (B; *, P < 0.05, **, P < 0.01, ***, P < 0.001, ****, P < 0.0001). Cross (†) indicates deceased mice on given day. DPI, days p.i. Mantel–Cox (log-rank) test was performed to determine statistical significance for survival data. P values and number of mice are indicated in the panels.

with stem Abs in close proximity to the HA receptor binding site, completely blocked activation (Fig. 6 A).

Having established a robust system for measuring stem Ab–based FcγR coupled innate cell activation we next examined whether the anti-NA activity of stem-specific Abs enhances activation. After incubating reporter cells overnight with virus–Ab mixtures, cellular activation was enhanced twofold by del24 relative to WT or ins20 virus, implicating NA-based inhibition of FcγR-based activation. Consistent with this observation, adding Food and Drug Administration–approved NA inhibitors (oseltamivir [OSL] and zanamivir [ZNV]) increased reporter cell activation in all circumstances (Fig. 6 B, top). The greatest enhancement was observed with WT and ins20 viruses in the presence of NA inhibitors (Fig. 6 B). Curiously, despite what should be complete NAI with the drugs, activation remained less than observed with del24 or del24 plus NA inhibitors, which achieved maximal activation. NA inhibitors also enhanced anti-HA stem Ab–dependent innate cell activation by MDCK SIAT1 cells infected with WT or and NA stalk variant viruses. Interestingly, however, NA stalk length did not modulate activation (Fig. 6 B, bottom).

Our interpretation of these data is that first, virus or cell-surface NA interferes with FcγR-based cell activation by cleaving SA on reporter cells, which can be blocked with NA inhibitors. Second, stem Ab–based steric effects on NAI are far less sensitive on infected cells versus virus, probably due to the relaxed orga-

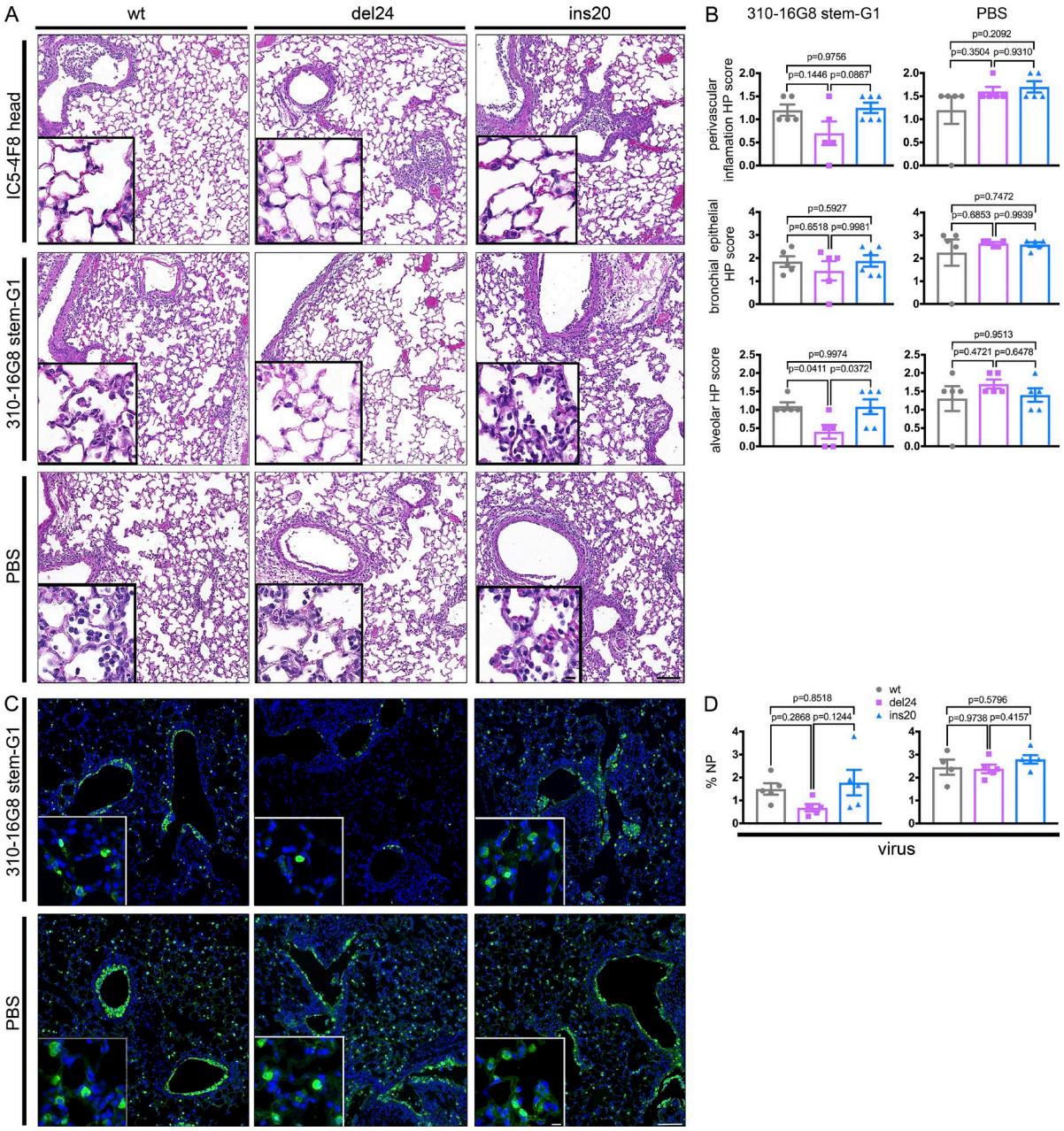

Figure 5. **Pathogenesis modulated by anti-stem Abs is dependent on NAI.** We passively transferred mice (n = 5–6/group, 5 mg/kg) with stem-specific mAb 310-16G8, head-specific mAb IC5-4F8, or PBS. 4 h after transfer, we infected mice intranasally with pathologically equal doses of WT, del24, and ins20 viruses. 4 d after challenge, we collected lungs and stained sections with hematoxylin (dark purple, nucleoli) and eosin (pink/red, cytoplasm) to visualize lung tissue damage and immune cell infiltration. **(A)** Representative lung section fields of mice infected with indicated viruses and treated as indicated. Bars, 100 µm (large fields); 10 µm (insets). **(B)** Quantitation of histopathogical (HP) changes. One-way ANOVA with Tukey's multiple comparisons was performed to determine statistical significance, with P values indicated in the panels. **(C)** Representative fields showing influenza NP expression revealed by immunofluorescence. Bars, 100 µm (large fields); 10 µm (insets). **(D)** Quantitation of NP staining using Bitplane Imaris 9.1 software to determine the fraction of infected cells using DNA staining to identify all cellular nuclei for normalization of cell number. Error bars indicate the SD of duplicate-triplicate samples acquired in two independent experiments. One-way ANOVA with Tukey's multiple comparisons was performed to determine statistical significance, with P values indicated in the panels.

nization of HA and NA spikes on the cell surface relative to the highly organized geometry on virions.

Discussion

HA stem–specific Abs are perhaps the most promising approach for improving the duration and effectiveness of influenza vaccination. It is therefore important to better understand how anti-stem Abs provide in vivo protection. Evidence from mouse passive Ab transfer studies supports a critical role for FcγRs in protection at lower (i.e., more physiological) stem Ab concentrations, implicating innate cell mechanisms. These could include NK cell–mediated killing of infected cells (Bar-On et al., 2013), macrophage clearance of virus, and cytokine/chemokine secretion by any of the many type of FcγR-expressing cells.

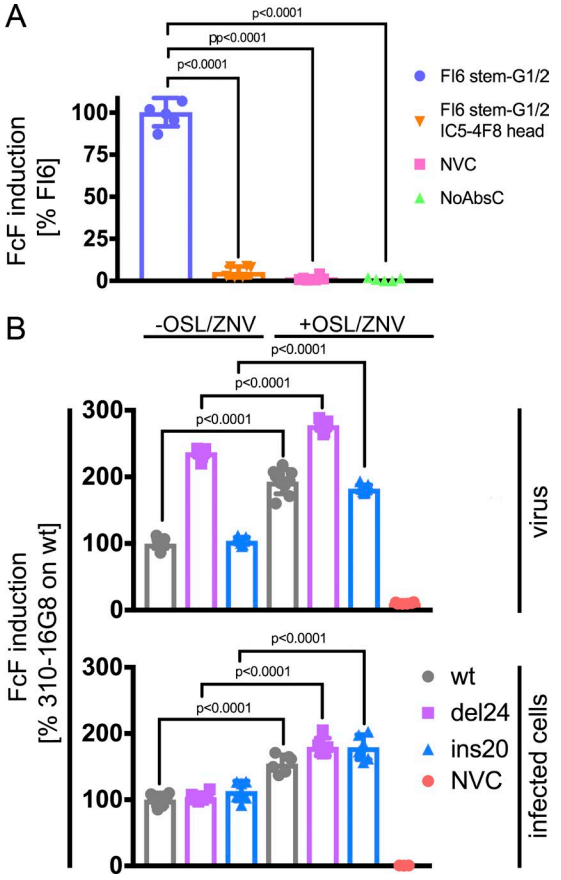

Figure 6. **NAI governs anti-stem HA Fc–mediated cellular activation by the virus but not infected cells. (A)** We infected MDCK SIAT1 cells with PR8 and at 5.5 h p.i. added the mAbs indicated and Jurkat FcγR reporter cells. After overnight incubation, we measured luciferase expression to gauge cell activation. 100% activation is defined by FI6 mAb alone. Error bars indicate the SD of triplicates samples acquired in two independent experiments ($n = 6$). **(B)** In the top graph, we preincubated WT, del24, or ins20 viruses (normalized by HAU) with the 16G8 anti-stem mAb and added Jurkat reporter cells in the presence or absence of OSL and ZNV. In the bottom graph, we infected cells at equal MOI with the viruses indicated and at 5–6 h p.i. added 16G8 and Jurkat reporter cells in the presence and absence of the OSL/ZNV. After overnight incubation, we measured luciferase expression to gauge cell activation. 100% activation is defined by FI6 mAb alone. Error bars indicate the SD of triplicate samples acquired in two independent experiments. One-way ANOVA with Tukey's multiple comparisons was performed to determine statistical significance, with P values indicated in the panels. FcF, fragment crystallizable–mediated function; NoAbsC, no Abs control; NVC, no virus control.

Here, we demonstrate a potentially critical role for NA in the antiviral activity of HA-specific Abs. By modulating the anti-NA effect of stem Abs using NA stalk–deleted and extended viruses, we could show that stem-binding Abs inhibit NA activity against large substrates, thereby blocking nascent virus release from infected cells. This phenomenon was reported previously (Yamayoshi et al., 2017), but the mechanism has not been defined.

Our findings have interesting implications for the organization of glycoproteins on the virion surface. We unequivocally demonstrate that anti-stem Abs have sufficient access to HA on intact virions to inhibit NA activity, extending cryo-EM–based observations that Abs can access HA stem on intact virions (Wasilewski et al., 2012; Harris et al., 2013; Williams et al., 2017). Examination of the Ab NAI titration curves (Fig. 2) reveals several intriguing features.

First, in agreement with Rajendran et al. (2017), ∼25% of NA activity remains at anti-stem Ab saturation. Since removing the Fc domain approximately doubles the resistant NA fraction, this suggests the existence of three NA populations: one sufficiently close to HA to be inhibited by F(ab′)2, another that requires intact Ab, and a third that is too distant to be affected. As NA is generally present in clusters on the virion surface (Harris et al., 2006; Calder et al., 2010; Wasilewski et al., 2012), the Ab resistant fraction may represent NA active sites at the interior regions of clusters. Decreasing stalk length reduces the intact Ab resistant fraction by ∼50%. This may be due either to simple steric effects of lowering the active site or, intriguingly, by an alteration in the geometrical relationship between HA and NA on the virion surface, perhaps due to a decrease in NA cluster size.

Second, as NA stalk length increases, the amount of anti-stem Ab needed to block NA activity increases up to 20-fold, despite stalk length having no apparent effect on anti-HA binding to virions. As the Ab concentration increases, monovalent interactions will be favored, perhaps enabling more Abs bound per NA cluster, thus increasing the reach of stem-bound Abs.

In as much as the in vivo activity of stem-binding Abs is based on FcγR ligation (DiLillo et al., 2014, 2016; Mullarkey et al., 2016), such activities would not be expected to contribute to Ab-based protection in vivo. Consistent with this conclusion, we only detected up to threefold decrease in viral replication in stem Ab–treated mice, despite a clear protective effect. While in vivo viral replication was shown to correlate with stem Ab dose, protection was also reported at low doses. In such a case, viral replication can be reduced less than 10-fold (DiLillo et al., 2014; Kallewaard et al., 2016) while still completely protecting against mortality.

Remarkably, extending the NA stalk greatly reduced the protective effect of anti-HA stem mAbs, strongly implicating NAI in Ab-mediated protection in our experimental system (Figs. 4 and 5). Conversely, shortening the NA stalk reduced immune alveolar inflammation and lymphocyte infiltration and increased protection at high virus doses. These data are consistent with the conclusion that in vivo protection mediated by anti-stem Abs is based on NAI. While we could show that NA inhibits FcγR reporter cell activation, it is important to note that the NAI-based protective effects of anti-stem Abs could be based on a multiple mechanisms, including enhancing Fc-based innate cell functions (virion phagocytosis, NK cell killing/cytokine release) and inhibition of virion release from infected cells and other SA containing surfaces.

NAI of FcγR expressing cells is consistent with the finding that anti-HA head-specific Abs block NK cell Ab-dependent cellular cytotoxicity (ADCC) killing while NA-specific Abs enhance it (He et al., 2016). The simplest explanation for this phenomenon is that HA-mediated binding to SA on innate immune cells is required for cell activation. Indeed, Ab-independent NK cell recognition of IAV-infected cells requires HA binding to the NK-activating receptors NKp46, NKp44 (Mandelboim et al., 2001), 2B4, or NTB (Duev-Cohen et al., 2016), and viral NA inhibits this activation (Bar-On et al., 2013). Because the Jurkat FcγR reporter cells we and others (He et al., 2016) have used are not known to

express NK-activating receptors, it appears that their requirement for HA binding in Ab-based activation reflects HA binding to other cell-surface ligands.

NA blockade of Ab-dependent and independent innate immune cell anti-IAV activity supports the possibility that NA inhibitors owe their clinical efficacy to more than just blocking virus release, as suggested by Bar-On et al. (2013). Further, if innate immune effector functions limit IAV transmission, then NA-mediated antagonism could contribute to NA evolution, with NA stalk length possibly being under selective pressure by virtue of its functional interaction with HA stem–specific Abs. Pragmatically, the ability of NA inhibitors to enhance FcγR-mediated innate immune cell activation of stem Abs bound to viruses or infected cells suggests the possible clinical synergism between NA inhibitors and anti-stem mAbs in humans. Such an idea is supported by the enhanced in vivo protective effect of BN HA–oseltamivir combined treatment (Nakamura et al., 2013).

Materials and methods

Animals

We purchased C57BL/6 mice from Taconic Farm. We used female 8–12-wk-old mice randomly assigned to experimental groups. We held mice under specific pathogen–free conditions. All animal procedures were approved and performed in accordance with National Institute of Allergy and Infectious Diseases Animal Care and Use Committee Guidelines. For passive transfer, we weighed and injected mice with 5 mg/kg of each mAb in 400 µl sterile saline solution intraperitoneally. For mouse infections, we anesthetized mice with isoflurane (3.5%) and injected 25 µl virus intranasally (WT, 3.5×10^3; del24, 5×10^3; and ins20, 4×10^3) diluted in sterile saline supplemented with 0.1% BSA. We recorded weight for 14 d and euthanized mice when mice reached 30% weight loss. We excluded mice ($n = 2$) that showed no signs of infection and weight loss compared with the rest of the animals in a given experiment. When needed, we harvested and homogenized lungs and determined viral titers.

Cell lines and viruses

We cultured MDCK SIAT1 cells in DMEM (Gibco) supplemented with 8% FBS (HyClone) and 500 µg/ml gentamicin (Quality Biologicals) and 500 µg/ml geneticin (Gibco) at 37°C and 5% CO_2. We cultured human embryonal kidney 293T cells in DMEM supplemented with 8% FBS (HyClone) and 500 µg/ml gentamicin at 37°C and 5% CO_2. We used Expi293 cells (Thermo Fisher) for BN HA stem mAb expression. We propagated and cultured the cells as recommended by the manufacturer. We employed the following viruses in this study: A/Puerto Rico/8/34/H1N1 (Walter Gerhart), A/California/07/2009/H1N1, A/Texas/50/2012/H3N2, A/Switzerland/9715293/2013/H3N2, A/Hong Kong/4801/2014/H3N2, A/Puerto Rico/8/34/H1N1/ins20 NA, A/Puerto Rico/8/34/H1N1/del24 NA, A/Hong Kong/1/68 (H3N2), chimeric HA influenza virus with HA head domain from the A/Vietnam/1203/04 (H5N1), HA stem domain from PR8 (Hai et al., 2012), and NA from A/Udorn/72/H3N2 (cH5/1N2). We generated the NA stalk viruses by cotransfection of the eight influenza gene–coding plasmids (provided by Dr. Adolfo Garcia-Sastre, Icahn School of Medicine at Mt. Sinai, New York, NY) as published previously (Kosik et al., 2018). To generate deletion in the NA stalk while preserving cysteine at position 49, we performed mutagenic overlapping PCR with forward primer 5′-AGCCATTCATGCAAGGACACAACTTCAGTGATATTAACC-3′ and reverse primer 5′-TGTGTCCTTGCATGAATGGCTAATCCATATTGAG-3′. We used the pDZ-NA plasmid as a template along with Kod Hot start DNA polymerase (Millipore Sigma). For the NA insertion variant, we used 5′ phosphorylated forward primer (5′-AATTTTCTTACTGAAAAAGTTGTTGCTGGGAAGGACACAACTTCAGTGATATTAACCG-3′) containing 30 nucleotides from the NA stalk region of the A/Goose/Guangdong/1/96/H5N1 (AF144304) and reverse primer (5′-GGTATTGCTGATGTTGACATATGTTTGATTTACCCAGGTGCTATTTTTATAGGTAATG-3′) containing 15 nucleotides from NA stalk region of the A/Goose/Guangdong/1/96/H5N1 and 15 nucleotides from A/WSN/33/H1N1 (LC333187). We followed the manufacturer's recommendations to PCR mutagenize the pDZ-NA open reading frame. We recircularized linearized plasmid PCR products with a Rapid DNA Ligation Kit (Roche) and transformed plasmids into DH5α-competent cells (Thermo Fisher). After purification with plasmid purification (Qiagen), we sequenced plasmids. To rescue chimeric cH5/1N2, we cotransfected plasmid harboring chimeric HA with N2 plasmid (provided by Dr. Peter Palese [Icahn School of Medicine at Mount Sinai, New York, NY] and Dr. Kanta Subbarao [National Institute of Allergy and Infectious Diseases, National Institutes of Health, Bethesda, MD] respectively) combined with PR8 core plasmids and followed as described above. For the self-reporting NS1-mCherry expressing virus, we first modified reverse genetics system pDZ plasmid as follows.

We cloned NS1-mCherry into the pDZ vector plasmid in several steps. First, we amplified NS1 by PCR with primers NS-5′-SapI (5′-GCTCTTCAGGGAGCAAAAGCAGGGTGACAAAG-3′) and NS1-mCherry bot (5′-GCCGCTGCCATCGATGCCAACTTCTGACCTAATTGTTC-3′). We PCR amplified mCherry with primers NS1-mCherry top (5′-TGGCATCGATGGCAGCGGCATGGTGAGCAAGGGCGAGGAG-3′) and mChe-2A-NEP bot (5′-AGGCTAAAGTTGGTCGCGCCACCGCTGCCCTTGTACAGCTCGTCCATGCC-3′). We PCR amplified NEP with primers NEP–exon 1 (5′-GAAAACCCGGGCCCGATGGATCCAAACACTGTGTCAAGCTTTCAGGACATACTGCTGAGGATGTCAA-3′), which encodes NEP exon 1 fused to exon 2, and primer NS-3′-SapI (5′-GCTCTTCTATTAGTAGAAACAAGGGTGTTTT-3′). After all amplification steps, we dissected PCR fragments from an agarose gel and purified with the QIAquick gel extraction kit (Qiagen). We extended the NEP fragment further using primers 2A-NEP (5′-GGCGCGACCAACTTTAGCCTACTGAAACAGGCGGGCGATGTGGAAGAAAACCCGGGCCCGATGGA-3′) and NS-3′-SapI, which added the "self-cleaving" 2A sequence of porcine teschovirus. We diluted purified mCherry and 2A-NEP fragments 1:50 and joined with splice-overlap extension PCR using primers NS1-mCherry top and NS-3′-SapI. We digested the NS1 fragment and mCherry-2A-NEP fragment with SapI and ClaI restriction enzymes and ligated to pDZ vector digested with SapI. The final construct codes for NS1 fused to a six amino acid linker (GIDGSG) fused to mCherry followed by the 2A sequence and both exons of NEP. We sequenced the final plasmid and used it instead of pDZ-NS in rescue as described above. We propagated viruses in 10-d-old embryonated chicken eggs for 48 h, and we

stored allantoic fluid at −80°C. For virus purification, we clarified allantoic fluid at 4,700 rounds per minute (RPM) for 10 min, and pelleted virus by centrifugation for 2 h at 27,000 RPM. We incubated pellets overnight in 2 ml PBS with calcium and magnesium (PBS++) and purified virus by centrifugation on a discontinuous 15–60% sucrose gradient, collecting virus at the interface, and pelleting 34,000 RPM for 2 h. After resuspending the pellet in 500 µl PBS++ overnight, we measured total viral protein with the DC Protein Assay (Bio-Rad).

Viral sequencing

We extracted influenza virus genomic RNA from clarified allantoic fluid using the QIAamp Viral RNA Mini Kit (Qiagen) according to the manufacturer's protocol. We amplified complete genomes with a multiplex RT-PCR protocol using SuperScript III One-Step RT-PCR System with Platinum Taq DNA Polymerase and primers targeting conserved 5′ and 3′ sequences in the viral RNA (Zhou and Wentworth, 2012). Libraries for next-generation sequencing were constructed from 1-ng amplified genomes using the Nextera XT DNA Library Preparation Kit (Illumina) and sequenced using the MiSeq Reagent Kit v2 on the MiSeq Platform (Illumina). Viral sequences were assembled de novo using a high-throughput assembly pipeline (Mena et al., 2016), and variant statistics were assembled using custom perl scripts.

Antibodies

We produced the human IgG1 BN HA stem mAbs 310-16G8, 310-18F8, FI6, and CR8020 (Ekiert et al., 2011; Whittle et al., 2014) by transient plasmid (provided by Dr. Adrian McDermott, Vaccine Research Center, National Institutes of Health, Bethesda, MD) cotransfection in the Expi293 Expression System (Thermo Fisher) following the manufacturer's recommendations. The IC5-4F8 Sb–specific, H2-6A1 Sa–specific, HA2-specific mAb RA5-22, NP-specific mAb HB65, rabbit anti–C-terminal NP polyclonal serum 2364 (487-498aa), NA-specific NA2-1C1 mAb, NA2-10E10 mAb, rabbit anti–C-terminal NA polyclonal serum, and TW1.3 vaccinia-specific mAb were prepared in the laboratory as published previously (Yewdell et al., 1981; Kosik and Yewdell, 2017). We prepared the polyclonal anti-HK68 mouse serum by single dose intramuscular immunization (5 µg) of whole purified UV-inactivated virus. We collected serum 21 d after immunization. After heat inactivation at 56°C for 30 min, we stored serum at −80°C.

Virus hemagglutination titer

We diluted allantoic fluid containing half-log serial dilutions of virus in Dulbecco's PBS (DPBS) in a round-bottom 96-well plate (Greiner Bio-One). We combined 50 µl of the virus dilutions with 50 µl 0.5% turkey RBCs and incubated at 4°C for 1 h. We determined HA titer as reciprocal of highest dilution providing full hemagglutination. We tested all viruses in triplicate in two independent experiments.

In-cell immunoassay and median tissue culture infectious dose ($TCID_{50}$)

We seeded MDCK SIAT1 cells (10,000–50,000 per well) in a 96-well plate (Costar). The following day we washed cells with DPBS twice and added virus diluted in infection media (MEM medium [Gibco] containing 0.3% BSA [fraction V; Roche], 10 mM HEPES [Corning], 500 µg/ml gentamicin [Quality Biologicals], and 1 µg/ml TPCK trypsin [Worthington]). At the times p.i. indicated, we fix-permeabilized the cells with 100% ice-cold methanol for 20 min. We washed the cells with DPBS and added 30 µl HB65 anti-NP mAb or/and NA2-1C1 anti-NA mAb (1 µg/ml) diluted in Odyssey Blocking Buffer PBS (OBB; Li-Cor) for 1 h at room temperature. We washed the plate with DPBS containing 0.05% NP-40 (Thermo Fisher) twice and added IRDye 800CW goat anti-mouse or IRDye 680RD goat anti-rabbit secondary Ab (Li-Cor) 1,000× diluted in OBB. After 1-h incubation at room temperature, we washed the plate twice as described above with one final milliQ water washing step.

For $TCID_{50}$ determination, we prepared half-log_{10} dilutions of the virus sample in infection media. We transferred virus dilutions in replicates of eight to MDCK SIAT1 cells in a 96-well plate (Costar). At 18 h p.i., we proceeded as described above. We used the HB65 anti-NP-specific mAb along with 1,000-fold diluted IRDye 800CW goat anti-mouse secondary Abs to detect IAV-positive wells. We scanned the plates using a near-infrared imaging system (OdysseyCLx; Li-Cor). We used ImageStudioLite software to quantify the measured signal. For the positive/negative threshold, we used doubled averaged signal of eight uninfected wells. We used the Spearman and Karber method to calculate $TCID_{50}$. For quantification of NA and NP expression, we subtracted the average signal of four uninfected wells. We plotted $TCID_{50}$, NA, and NP signal data using GraphPad Prism7.

Protein gels and immunoblotting

We diluted freshly purified virus samples (25 µg/ml) in DPBS and combined three volumes of virus with one volume of NuPAGE LDS Sample Buffer (4×; Thermo Fisher) containing 100 mM dithiothreitol. We heated samples at 70°C for 10 min, cooled them on ice, and loaded 5 µl (100 ng) of the sample on NuPAGE 4–12% Bis-Tris Protein Gel (Thermo Fisher), separating proteins by electrophoresis with Chameleon Pre-Stained Protein Ladder (Li-Cor) on 4–12% Bis-Tris Gels (Invitrogen) at 150 V for 90 min. We transferred proteins to nitrocellulose membranes using an iBlot device at P3 setting for 7 min. We blocked membranes with OBB for 1 h at room temperature and incubated with rabbit anti–C-terminal NA polyclonal serum (5,000× dilution) and RA5-22 mAb (1 µg/ml) diluted in OBB. We washed the membrane in DPBS containing 0.05% NP-40 three times and incubated for 1 h at room temperature with IRDye 800CW goat anti-mouse or IRDye 680RD goat anti-rabbit secondary Ab (Li-Cor) diluted 20,000-fold in OBB. We washed the membrane three times with one additional milliQ water washing step. We scanned the membrane with the near-infrared imaging system (OdysseyCLx). We used ImageStudioLite software to quantify signal and plotted the data using GraphPad Prism7 software.

ELISA

We coated ELISA plates (half-area 96-well; Greiner Bio-One) with 10 ng of respective purified IAV diluted in DPBS (50 µl per well). After overnight incubation at 4°C, we washed plates three times with DPBS supplemented with 0.05% Tween-20. We serially di-

luted (half-log dilutions) Abs starting from 10 to 100 nM in 1% BSA in DPBS and added 50 µl to plates for 90 min at 37°C. After extensive washing with DPBS+0.05% Tween-20, we detected bound Abs by incubating plates with 50 µl HRP-conjugated rat anti-mouse IgG kappa chain (Southern Biotech) for 1 h at room temperature. We washed ELISA plates with DPBS+0.05% Tween-20 and incubated with SureBlue TMB Microwell Peroxidase Substrate (KPL) for 5 min at room temperature. We stopped the enzymatic reaction by adding HCl. We measured absorbance at 450 nm (A_{450}) on a Synergy H1 plate reader (Biotek) and calculated the dissociation constant (K_d) from dilution curves using GraphPad Prism 6 software to fit one-site binding.

ELLA

We performed ELLA as described previously (Kosik and Yewdell, 2017). We avoided Tween-20 in all steps to preserve virion integrity. We determined the virus dilution yielding an A_{450} between 1 and 1.5. We also normalized samples to a similar hemagglutination unit (HAU) contents. We coated half-area 96-well ELISA plates (Greiner Bio-One) with 50 µl fetuin solution in DPBS (25 µg/ml) overnight at 4°C. We diluted Abs initially to 200 nM and then serially by 3.1-fold. We preincubated 25 µl Ab dilutions with 25 µl virus in sample diluent (DPBS, 1% BSA) for 60 min at 37°C and then added the samples to a fetuin-coated plate for 18–22 h at 37°C. We washed plates extensively with washing buffer (DPBS, 0.05% Tween-20) and then added 50 µl peanut-HRP (Sigma-Aldrich) diluted 1,000-fold in sample diluent for 1 h at room temperature in the dark. After washing, we detected and read the plate as for ELISA. To liberate HA and NA from the virion, we added 0.5% Triton X-100 in sample diluent for 10 min at room temperature and then followed the standard ELLA procedure. We normalized data by signal in the absence of mAb. We plotted data with GraphPad Prism7 software and fit nonlinear regression curves using the dose-response inhibition model.

Attachment inhibition (AI) assay

We performed AI assay as described previously (Kosik and Yewdell, 2017). Briefly, we coated black, half-area, high-binding 96-well plates (Nunc) with 50 µl fetuin in DPBS (25 µg/ml) overnight at 4°C. We determined the highest dilution of the virus yielding sufficient signal. We diluted mAbs or H3N2-specific mouse sera initially to 200 nM or 20-fold, respectively, and then serially by half-log_{10} steps. We mixed Abs with diluted allantoic fluid and incubated for 60 min at 37°C. We then transferred 50 µl Ab-virus mixture to washed fetuin-coated plates, incubated for 1 h at 4°C, and removed free virus by washing six times with DPBS. We added 50 µl of 200 µM MUNANA in 33 mM MES, pH 6.5, with 4 mM $CaCl_2$ and incubated for 1 h at 37°C. We measured fluorescence (excitation [Ex] = 360 nm; emission [Em] = 450 nm) using a Synergy H1 plate reader (Biotek). The signal in the absence of Ab defines 100% attachment. We fitted nonlinear regression curves using the dose-response inhibition model with GraphPad Prism7 software.

Flow cytometry

For flow cytometry–based neutralization assay, we seeded 50,000 MDCK SIAT1 cells to 96-well tissue culture–treated plates (Costar). The next day, we preincubated (at 37°C for 1 h) 50 µl of half-log_{10} serially diluted Abs with 50 µl of the respective mCherry-expressing or WT virus at multiplicity of infection (MOI) = 0.05–0.1 per well. We diluted Abs and virus in infection media. We transferred virus-Ab mixture to washed MDCK SIAT1 cells and incubated samples at 37°C for the time indicated (4–5 h/18 h). We washed cells twice with DPBS and added 30 µl of 0.005% trypsin-EDTA (Gibco) for 20 min, 30 µl BSA, and then 30 µl 1.6% paraformaldehyde (Electron Microscopy Science) for 20 min. We sedimented cells by centrifugation at 1,500 RPM for 5 min and washed samples with BSA two times. We also included uninfected and samples without Ab as controls. In the case of WT virus (HK68 H3N2), we fix-permeabilized the cells with a Foxp3/Transcription Factor Staining Buffer Set (Thermo Fisher) as recommended by the manufacturer. We washed the cells once, incubated with 1,000-fold–diluted NP mAb (HB65-AF647) for 30 min, and washed and resuspended with BSA solution. For comparing the access of the HA stem epitope in the context of cell-expressed HA, we seeded 2.5 million MDCK SIAT1 cells per T25 tissue culture flasks and infected cells the next day with viruses MOI = 1) diluted in infection media. At 18 h p.i., we washed cells twice with DPBS, detached from the flask with trypsin-EDTA (Gibco), and combined with half-log_{10} serial dilutions of mAbs. We incubated samples at 37°C for 1 h, washed with BSA and combined with 50 µl 200× diluted mouse anti-human FITC (Pharmingen) or 5,000× diluted donkey anti-mouse AF488 (Jackson Immunology). We washed samples three times, fixed with 4% paraformaldehyde for 20 min, washed three times again, and resuspended in BSA. Samples were analyzed using a BD LSRFortessa X-20 instrument. Analysis was performed using FlowJo software (TreeStar). We normalized the frequencies of mCherry/NP-positive cells by the non-Ab–treated samples and fitted nonlinear regression curves using the dose-response inhibition model for neutralization assay or one-site binding for epitope access assay with GraphPad Prism7 software.

Cell-surface virus elution assay

We seeded 20,000 MDCK SIAT1 cells to 96-well tissue culture–treated plates (Costar). The next day, we washed cells twice with DPBS and infected cells with viruses (MOI = 5) diluted in infection media without trypsin. At 4 h p.i., we washed cells with DPBS twice and added 50 µl of serially diluted (fourfold) mAbs. At 10 h p.i., we transferred 40 µl of the supernatant to a round-bottom 96-well plate (Costar) and pelleted the cells at 4,700 RPM for 10 min. We gently transferred 30 µl of the supernatant to a half-area black 96-well plate (Costar) and combined with 30 µl of 200 µM MUNANA in 33 mM MES, pH 6.5, with 4 mM $CaCl_2$. We incubated the samples for 1 h at 37°C. We measured fluorescence (Ex = 360 nm; Em = 450 nm) using a Synergy H1 plate reader. The signal in the absence of Ab defines 100% elution. We fitted nonlinear regression curves using the dose-response inhibition model with GraphPad Prism7 software.

ADCC assay

We seeded 10,000 MDCK SIAT1 cells to 96-well white tissue culture–treated plates (Costar). The following day, we washed cells twice with DPBS and infected cells with viruses (MOI = 5) as described above. At 6 h p.i., we combined 25 µl of 200 nM mAb

with 25 µl of ADCC-RL cells (Jurkat cell line expressing luciferase gene under control of the NFAT response element and stably expressing human FcγRIIIa V158; Promega) containing 50,000 in RPMI 1640 medium with 4% low-IgG serum (Promega). We added the Ab-ADCC-LR mixture onto the MDCK SIAT1 cells (effector cells:target cells = 5:1). After overnight incubation at 37°C in 5% CO_2, we added 50 µl of Bright-Glo Luciferase Assay lysis/substrate buffer (Promega) and measured luminescence within 5 min using a Synergy H1 plate reader (Biotek). Alternatively, we combined 25 µl of respective virus containing 40 HAU with 25 µl of 300 nM mAb, incubated virus-Ab mixtures at 37°C for 1 h and added 25 µl ADCC-LR (50,000). We incubated mixtures overnight at 37°C in 5% CO_2 and measured the luminescence signal as described above. We included samples in the absence of the virus as negative controls. When indicated, in addition to mAbs, a mixture of oseltamivir phosphate (American Radiolabeled Chemicals) and ZNV (Moravek) was added to samples at a 2.5 µM final concentration. We normalized the data to the signal of FI6 or 310-16G8 on WT PR8 virus. We plotted the data using GraphPad Prism7 software.

NA catalytic activity

We diluted freshly purified viruses (~2 µg/ml) in 33 mM MES, pH 6.5, with 4 mM $CaCl_2$ to contain equal NA amounts based on multiple immunoblot experiments. We twofold serially diluted MUNANA in the same buffer starting at 500 µM and preincubated virus solutions and MUNANA dilutions at 37°C for 30 min to equilibrate temperatures. We combined 20 µl virus with 20 µl of the respective MUNANA dilution in a half-area 96-well plate (Costar) and incubated the samples at 37°C to generate fluorescent product of the catalytic reaction. After 60-min incubation, we measured fluorescence generated (Ex = 360 nm; Em = 450 nm) using a Synergy H1 plate reader (Biotek). We measured background fluorescence of the respective MUNANA dilutions and subtracted it from samples. In parallel, we diluted 4-MU (the catalytic product of MUNANA cleavage) serially (twofold), and we measured fluorescence as described above. We generated a calibration curve by fitting linear regression in GraphPad Prism7 software, and we interpolated the amount of 4-MU produced by viruses. We fit the data to Michaelis–Menten regression in GraphPad Prism7 software.

RBC virus release assay

We measured relative NA activity of the viruses in allantoic fluid. We normalized samples based on equal NA activity (determined by MUNANA), and we diluted samples serially (twofold) in PBS++ and combined 50 µl of the virus with 50 µl of 0.5% turkey RBCs diluted in PBS++. We incubated plates at 4°C for 1 h, recorded the HA titer, and transferred the plates to 37°C. We recorded complete elution every 30 min for 7 h. We divided complete elution dilution at time indicated by HA titer to normalize for viral particles amount. We transformed the data as the percentage of WT PR8 elution at 7 h. We plotted the data in GraphPad Prism7 software.

2D cryo-EM

For cryo-EM, we froze 3.5 µl viral suspension on glow-discharged 20-mesh R2/2 Quantifoil Cu grids (Quantifoil) using a Leica EM GP plunge. We blotted the grids for 2 s at 99% relative humidity using 1-s wait and drain times, respectively. We mounted plunge frozen grids in autogrids assembly and imaged under cryo conditions at 300 kV on Titan Krios (Thermo Fisher Scientific) using a Falcon II direct electron detector. We collected cryo 2D images using a volta phase plate for increased contrast at a nominal magnification of 29,000×, which corresponds to a pixel size of 2.87 Å with 1-micron defocus at a total dose of 12 $e^-/Å^2$.

Histopathology and immunohistochemistry

We infected mice intranasally with PR8 influenza A WT, del24, or ins20 NA variant viruses (3,000–5,000 $TCID_{50}$). At 4 d p.i., we sacrificed the mice and inflated lungs by 10% buffered formalin through the trachea. We fixed lungs overnight and processed them for paraffin embedding. We made serial sections at 5 µm thickness and stained every 10th slide using hematoxylin and eosin. We dewaxed the unstained and stained with influenza NP Ab (rabbit, 172) followed by Alexa Fluor 488–conjugated rabbit IgG (Jackson ImmunoResearch). We also counterstained with DAPI. We digitally scanned the light and fluorescence slides using an NDP NanoZoomer XR whole slide scanning system (Hamamatsu Photonics K.K.) and stored in ndpi format for further analysis. We used Imaris Image analysis software (Bitplane) to examine histopathology and influenza A NP–stained cells. We exported the analyzed data to Prism 7 software (GraphPad) for statistical analysis.

Online supplemental material

Fig. S1 shows AI comparison of anti-HA head and stem Abs, NAI in the context of detergent-dissociated HA and NA, NAI and VN activities of anti-stem mAbs on H3N2 IAV, a comparison of NAI activity of anti-stem and anti-NA mAbs, and amino acid sequence alignment of PR8 versus Udorn NA stalk regions. Fig. S2 shows (for the engineered PR8 NA stalk length variants) amino acid sequence alignment, 2D cryo-EM, Western blot analysis of NA mobility shift, relative quantification of virion-associated HA and NA, RBC elution, and in vitro and in vivo growth replication. Fig. S3 demonstrates that NA stalk length does not influence anti-stem mAb binding to virion or cell-expressed HA. Fig. S4 shows that NA stalk length does not influence NP intracellular expression or NA surface expression and that irrelevant anti-vaccinia virus Abs do not interfere with virion release from infected cells. Table S1 describes the enzymatic properties of the NA stalk length variants.

Acknowledgments

We thank Adrian McDermott for providing BN HA IgG1–expressing plasmids, Peter Palese for providing cH5/1-expressing plasmids, and Kanta Subbarao for providing pHH21-N2 IAV reverse genetic plasmid. We thank Glenys Reynoso for outstanding technical assistance.

This work was supported by the Division of Intramural Research of the National Institute of Allergy and Infectious Diseases.

The authors declare no competing financial interests.

Author contributions: Conceptualization, I. Kosik, D. Angeletti, M. Angel, and J.W. Yewdell; Methodology, I. Kosik, D. An-

geletti, M. Kosikova, H.D. Hickman, and J.W. Yewdell; Software, M. Angel; Validation, I. Kosik; Formal analysis, I. Kosik, D. Angeletti, M. Angel, K. Takeda, M. Kosikova, V. Nair, H. Xie, and J.W. Yewdell; Investigation, I. Kosik, J.S. Gibbs, D. Angeletti, M. Angel, K.T., M. Kosikova, V.N., and C.C. Brooke; Resources, H.D. Hickman, H. Xie, and J.W. Yewdell; Data curation, I. Kosik, M. Angel, K. Takeda, and M. Kosikova; Writing (original draft), I. Kosik, D. Angeletti, and J.W. Yewdell; Visualization, I. Kosik, K. Takeda, M. Kosikova, V. Nair, and J.W. Yewdell; Project administration, I. Kosik and J.W. Yewdell; Supervision, J.W. Yewdell; Funding acquisition, J.W. Yewdell.

Submitted: 23 August 2018
Revised: 3 November 2018
Accepted: 3 January 2019

References

Bar-On, Y., A. Glasner, T. Meningher, H. Achdout, C. Gur, D. Lankry, A. Vitenshtein, A.F.A. Meyers, M. Mandelboim, and O. Mandelboim. 2013. Neuraminidase-mediated, NKp46-dependent immune-evasion mechanism of influenza viruses. *Cell Reports.* 3:1044–1050. https://doi.org/10.1016/j.celrep.2013.03.034

Bi, Y., H. Xiao, Q. Chen, Y. Wu, L. Fu, C. Quan, G. Wong, J. Liu, J. Haywood, Y. Liu, et al. 2015. Changes in the Length of the Neuraminidase Stalk Region Impact H7N9 Virulence in Mice. *J. Virol.* 90:2142–2149. https://doi.org/10.1128/JVI.02553-15

Calder, L.J., S. Wasilewski, J.A. Berriman, and P.B. Rosenthal. 2010. Structural organization of a filamentous influenza A virus. *Proc. Natl. Acad. Sci. USA.* 107:10685–10690. https://doi.org/10.1073/pnas.1002123107

Chiu, C., A.H. Ellebedy, J. Wrammert, and R. Ahmed. 2015. B cell responses to influenza infection and vaccination. *Curr. Top. Microbiol. Immunol.* 386:381–398.

Chockalingam, A.K., D. Hickman, L. Pena, J. Ye, A. Ferrero, J.R. Echenique, H. Chen, T. Sutton, and D.R. Perez. 2012. Deletions in the neuraminidase stalk region of H2N2 and H9N2 avian influenza virus subtypes do not affect postinfluenza secondary bacterial pneumonia. *J. Virol.* 86:3564–3573. https://doi.org/10.1128/JVI.05809-11

Corti, D., J. Voss, S.J. Gamblin, G. Codoni, A. Macagno, D. Jarrossay, S.G. Vachieri, D. Pinna, A. Minola, F. Vanzetta, et al. 2011. A neutralizing antibody selected from plasma cells that binds to group 1 and group 2 influenza A hemagglutinins. *Science.* 333:850–856. https://doi.org/10.1126/science.1205669

Corti, D., E. Cameroni, B. Guarino, N.L. Kallewaard, Q. Zhu, and A. Lanzavecchia. 2017. Tackling influenza with broadly neutralizing antibodies. *Curr. Opin. Virol.* 24:60–69. https://doi.org/10.1016/j.coviro.2017.03.002

Cox, F., T. Kwaks, B. Brandenburg, M.H. Koldijk, V. Klaren, B. Smal, H.J. Korse, E. Geelen, L. Tettero, D. Zuijdgeest, et al. 2016. HA Antibody-Mediated FcγRIIIa Activity Is Both Dependent on FcR Engagement and Interactions between HA and Sialic Acids. *Front. Immunol.* 7:399. https://doi.org/10.3389/fimmu.2016.00399

DiLillo, D.J., G.S. Tan, P. Palese, and J.V. Ravetch. 2014. Broadly neutralizing hemagglutinin stalk-specific antibodies require FcγR interactions for protection against influenza virus in vivo. *Nat. Med.* 20:143–151. https://doi.org/10.1038/nm.3443

DiLillo, D.J., P. Palese, P.C. Wilson, and J.V. Ravetch. 2016. Broadly neutralizing anti-influenza antibodies require Fc receptor engagement for in vivo protection. *J. Clin. Invest.* 126:605–610. https://doi.org/10.1172/JCI84428

Doud, M.B., J.M. Lee, and J.D. Bloom. 2018. Quantifying the effects of single mutations on viral escape from broad and narrow antibodies to an H1 influenza hemagglutinin. *bioRxiv.* doi:10.1101/210468 (Preprint posted January 22, 2018)

Duev-Cohen, A., Y. Bar-On, A. Glasner, O. Berhani, Y. Ophir, F. Levi-Schaffer, M. Mandelboim, and O. Mandelboim. 2016. The human 2B4 and NTB-A receptors bind the influenza viral hemagglutinin and co-stimulate NK cell cytotoxicity. *Oncotarget.* 7:13093–13105. https://doi.org/10.18632/oncotarget.7597

Ekiert, D.C., R.H. Friesen, G. Bhabha, T. Kwaks, M. Jongeneelen, W. Yu, C. Ophorst, F. Cox, H.J. Korse, B. Brandenburg, et al. 2011. A highly conserved neutralizing epitope on group 2 influenza A viruses. *Science.* 333:843–850. https://doi.org/10.1126/science.1204839

Hai, R., F. Krammer, G.S. Tan, N. Pica, D. Eggink, J. Maamary, I. Margine, R.A. Albrecht, and P. Palese. 2012. Influenza viruses expressing chimeric hemagglutinins: globular head and stalk domains derived from different subtypes. *J. Virol.* 86:5774–5781. https://doi.org/10.1128/JVI.00137-12

Harris, A., G. Cardone, D.C. Winkler, J.B. Heymann, M. Brecher, J.M. White, and A.C. Steven. 2006. Influenza virus pleiomorphy characterized by cryoelectron tomography. *Proc. Natl. Acad. Sci. USA.* 103:19123–19127. https://doi.org/10.1073/pnas.0607614103

Harris, A.K., J.R. Meyerson, Y. Matsuoka, O. Kuybeda, A. Moran, D. Bliss, S.R. Das, J.W. Yewdell, G. Sapiro, K. Subbarao, and S. Subramaniam. 2013. Structure and accessibility of HA trimers on intact 2009 H1N1 pandemic influenza virus to stem region-specific neutralizing antibodies. *Proc. Natl. Acad. Sci. USA.* 110:4592–4597. https://doi.org/10.1073/pnas.1214913110

He, W., G.S. Tan, C.E. Mullarkey, A.J. Lee, M.M. Lam, F. Krammer, C. Henry, P.C. Wilson, A.A. Ashkar, P. Palese, and M.S. Miller. 2016. Epitope specificity plays a critical role in regulating antibody-dependent cell-mediated cytotoxicity against influenza A virus. *Proc. Natl. Acad. Sci. USA.* 113:11931–11936. https://doi.org/10.1073/pnas.1609316113

Henry Dunand, C.J., and P.C. Wilson. 2015. Restricted, canonical, stereotyped and convergent immunoglobulin responses. *Philos. Trans. R. Soc. Lond. B Biol. Sci.* 370:20140238. https://doi.org/10.1098/rstb.2014.0238

Impagliazzo, A., F. Milder, H. Kuipers, M.V. Wagner, X. Zhu, R.M. Hoffman, R. van Meersbergen, J. Huizingh, P. Wanningen, J. Verspuij, et al. 2015. A stable trimeric influenza hemagglutinin stem as a broadly protective immunogen. *Science.* 349:1301–1306. https://doi.org/10.1126/science.aac7263

Kallewaard, N.L., D. Corti, P.J. Collins, U. Neu, J.M. McAuliffe, E. Benjamin, L. Wachter-Rosati, F.J. Palmer-Hill, A.Q. Yuan, P.A. Walker, et al. 2016. Structure and Function Analysis of an Antibody Recognizing All Influenza A Subtypes. *Cell.* 166:596–608. https://doi.org/10.1016/j.cell.2016.05.073

Kosik, I., and J.W. Yewdell. 2017. Influenza A virus hemagglutinin specific antibodies interfere with virion neuraminidase activity via two distinct mechanisms. *Virology.* 500:178–183. https://doi.org/10.1016/j.virol.2016.10.024

Kosik, I., W.L. Ince, L.E. Gentles, A.J. Oler, M. Kosikova, M. Angel, J.G. Magadán, H. Xie, C.B. Brooke, and J.W. Yewdell. 2018. Influenza A virus hemagglutinin glycosylation compensates for antibody escape fitness costs. *PLoS Pathog.* 14:e1006796. https://doi.org/10.1371/journal.ppat.1006796

Krammer, F., A. Garcia-Sastre, and P. Palese. 2018. Is It Possible to Develop a "Universal" Influenza Virus Vaccine? Toward a Universal Influenza Virus Vaccine: Potential Target Antigens and Critical Aspects for Vaccine Development. *Cold Spring Harb. Perspect. Biol.* 10:a028845. https://doi.org/10.1101/cshperspect.a028845

Lees, W.D., D.S. Moss, and A.J. Shepherd. 2014. Evolution in the influenza A H3 stalk - a challenge for broad-spectrum vaccines? *J. Gen. Virol.* 95:317–324. https://doi.org/10.1099/vir.0.059410-0

Li, J., H. Zu Dohna, C.J. Cardona, J. Miller, and T.E. Carpenter. 2011. Emergence and genetic variation of neuraminidase stalk deletions in avian influenza viruses. *PLoS One.* 6:e14722. https://doi.org/10.1371/journal.pone.0014722

Lu, Y., J.P. Welsh, and J.R. Swartz. 2014. Production and stabilization of the trimeric influenza hemagglutinin stem domain for potentially broadly protective influenza vaccines. *Proc. Natl. Acad. Sci. USA.* 111:125–130. https://doi.org/10.1073/pnas.1308701110

Mallajosyula, V.V., M. Citron, F. Ferrara, X. Lu, C. Callahan, G.J. Heidecker, S.P. Sarma, J.A. Flynn, N.J. Temperton, X. Liang, and R. Varadarajan. 2014. Influenza hemagglutinin stem-fragment immunogen elicits broadly neutralizing antibodies and confers heterologous protection. *Proc. Natl. Acad. Sci. USA.* 111:E2514–E2523. https://doi.org/10.1073/pnas.1402766111

Mandelboim, O., N. Lieberman, M. Lev, L. Paul, T.I. Arnon, Y. Bushkin, D.M. Davis, J.L. Strominger, J.W. Yewdell, and A. Porgador. 2001. Recognition of haemagglutinins on virus-infected cells by NKp46 activates lysis by human NK cells. *Nature.* 409:1055–1060. https://doi.org/10.1038/35059110

Matsuoka, Y., D.E. Swayne, C. Thomas, M.A. Rameix-Welti, N. Naffakh, C. Warnes, M. Altholtz, R. Donis, and K. Subbarao. 2009. Neuraminidase stalk length and additional glycosylation of the hemagglutinin influence the virulence of influenza H5N1 viruses for mice. *J. Virol.* 83:4704–4708. https://doi.org/10.1128/JVI.01987-08

Mena, I., M.I. Nelson, F. Quezada-Monroy, J. Dutta, R. Cortes-Fernández, J.H. Lara-Puente, F. Castro-Peralta, L.F. Cunha, N.S. Trovão, B. Lozano-Du-

bernard, et al. 2016. Origins of the 2009 H1N1 influenza pandemic in swine in Mexico. *eLife.* 5:5. https://doi.org/10.7554/eLife.16777

Mullarkey, C.E., M.J. Bailey, D.A. Golubeva, G.S. Tan, R. Nachbagauer, W. He, K.E. Novakowski, D.M. Bowdish, M.S. Miller, and P. Palese. 2016. Broadly Neutralizing Hemagglutinin Stalk-Specific Antibodies Induce Potent Phagocytosis of Immune Complexes by Neutrophils in an Fc-Dependent Manner. *MBio.* 7:e01624-16. https://doi.org/10.1128/mBio.01624-16

Nakamura, G., N. Chai, S. Park, N. Chiang, Z. Lin, H. Chiu, R. Fong, D. Yan, J. Kim, J. Zhang, et al. 2013. An in vivo human-plasmablast enrichment technique allows rapid identification of therapeutic influenza A antibodies. *Cell Host Microbe.* 14:93–103. https://doi.org/10.1016/j.chom.2013.06.004

Okuno, Y., Y. Isegawa, F. Sasao, and S. Ueda. 1993. A common neutralizing epitope conserved between the hemagglutinins of influenza A virus H1 and H2 strains. *J. Virol.* 67:2552–2558.

Okuno, Y., K. Matsumoto, Y. Isegawa, and S. Ueda. 1994. Protection against the mouse-adapted A/FM/1/47 strain of influenza A virus in mice by a monoclonal antibody with cross-neutralizing activity among H1 and H2 strains. *J. Virol.* 68:517–520.

Rajendran, M., R. Nachbagauer, M.E. Ermler, P. Bunduc, F. Amanat, R. Izikson, M. Cox, P. Palese, M. Eichelberger, and F. Krammer. 2017. Analysis of Anti-Influenza Virus Neuraminidase Antibodies in Children, Adults, and the Elderly by ELISA and Enzyme Inhibition: Evidence for Original Antigenic Sin. *MBio.* 8:e02281-16. https://doi.org/10.1128/mBio.02281-16

Russ, G., E. Varekova, and B. Styk. 1974. Steric effects in the reaction of influenza virus neuraminidases with antibodies. *Acta Virol.* 18:299–306.

Russ, G., K. Poláková, F. Kostolanský, B. Styk, and M. Vancíková. 1987. Monoclonal antibodies to glycopolypeptides HA1 and HA2 of influenza virus haemagglutinin. *Acta Virol.* 31:374–386.

Styk, B., G. Russ, and K. Poláková. 1979. Antigenic glycopolypeptides HA1 and HA2 of influenza virus haemagglutinin. III. Reactivity with human convalescent sera. *Acta Virol.* 23:1–8.

Sun, Y., Y. Tan, K. Wei, H. Sun, Y. Shi, J. Pu, H. Yang, G.F. Gao, Y. Yin, W. Feng, et al. 2013. Amino acid 316 of hemagglutinin and the neuraminidase stalk length influence virulence of H9N2 influenza virus in chickens and mice. *J. Virol.* 87:2963–2968. https://doi.org/10.1128/JVI.02688-12

Sutton, T.C., E.W. Lamirande, K.W. Bock, I.N. Moore, W. Koudstaal, M. Rehman, G.J. Weverling, J. Goudsmit, and K. Subbarao. 2017. *In Vitro* Neutralization Is Not Predictive of Prophylactic Efficacy of Broadly Neutralizing Monoclonal Antibodies CR6261 and CR9114 against Lethal H2 Influenza Virus Challenge in Mice. *J. Virol.* 91:e01603–e01617. https://doi.org/10.1128/JVI.01603-17

Varecková, E., V. Mucha, S.A. Wharton, and F. Kostolanský. 2003. Inhibition of fusion activity of influenza A haemagglutinin mediated by HA2-specific monoclonal antibodies. *Arch. Virol.* 148:469–486. https://doi.org/10.1007/s00705-002-0932-1

Wasilewski, S., L.J. Calder, T. Grant, and P.B. Rosenthal. 2012. Distribution of surface glycoproteins on influenza A virus determined by electron cryotomography. *Vaccine.* 30:7368–7373. https://doi.org/10.1016/j.vaccine.2012.09.082

Whittle, J.R., A.K. Wheatley, L. Wu, D. Lingwood, M. Kanekiyo, S.S. Ma, S.R. Narpala, H.M. Yassine, G.M. Frank, J.W. Yewdell, et al. 2014. Flow cytometry reveals that H5N1 vaccination elicits cross-reactive stem-directed antibodies from multiple Ig heavy-chain lineages. *J. Virol.* 88:4047–4057. https://doi.org/10.1128/JVI.03422-13

Williams, J.A., L. Gui, N. Hom, A. Mileant, and K.K. Lee. 2017. Dissection of epitope-specific mechanisms of neutralization of influenza virus by intact IgG and Fab fragments. *J. Virol.* 92:JVI.02006-17. https://doi.org/10.1128/JVI.02006-17

Yamayoshi, S., R. Uraki, M. Ito, M. Kiso, S. Nakatsu, A. Yasuhara, K. Oishi, T. Sasaki, K. Ikuta, and Y. Kawaoka. 2017. A Broadly Reactive Human Anti-hemagglutinin Stem Monoclonal Antibody That Inhibits Influenza A Virus Particle Release. *EBioMedicine.* 17:182–191. https://doi.org/10.1016/j.ebiom.2017.03.007

Yassine, H.M., J.C. Boyington, P.M. McTamney, C.J. Wei, M. Kanekiyo, W.P. Kong, J.R. Gallagher, L. Wang, Y. Zhang, M.G. Joyce, et al. 2015. Hemagglutinin-stem nanoparticles generate heterosubtypic influenza protection. *Nat. Med.* 21:1065–1070. https://doi.org/10.1038/nm.3927

Yewdell, J.W., E. Frank, and W. Gerhard. 1981. Expression of influenza A virus internal antigens on the surface of infected P815 cells. *J. Immunol.* 126:1814–1819.

Zhou, B., and D.E. Wentworth. 2012. Influenza A virus molecular virology techniques. *Methods Mol. Biol.* 865:175–192. https://doi.org/10.1007/978-1-61779-621-0_11